


# Scaling Relationship of *In Vivo* Muscle Contraction Strength of Rabbits Exposed to High-Frequency Nanosecond Pulse Bursts

Technology in Cancer Research & Treatment  
 Volume 17: 1-10  
 © The Author(s) 2018  
 Reprints and permission:  
[sagepub.com/journalsPermissions.nav](http://sagepub.com/journalsPermissions.nav)  
 DOI: 10.1177/1533033818788078  
[journals.sagepub.com/home/tct](http://journals.sagepub.com/home/tct)  


Yan Mi, PhD<sup>1</sup>, Jin Xu, PhD<sup>1</sup>, Xuefeng Tang, MS<sup>1</sup>, Changhao Bian, MS<sup>1</sup>, Hongliang Liu, MS<sup>2</sup>, Qiyu Yang, MS<sup>3</sup>, and Junying Tang, PhD<sup>3</sup>

## Abstract

We studied the influence of various parameters of high-frequency nanosecond pulse bursts on the strength of rabbit muscle contractions. Ten unipolar high-frequency pulse bursts with various field intensities  $E$  (1 kV/cm, 4 kV/cm, and 8 kV/cm), intraburst frequencies  $f$  (10 kHz, 100 kHz, and 1 MHz), and intraburst pulse numbers  $N$  (1, 10, and 100) were applied using a pair of plate electrodes to the surface skin of the rabbits' biceps femoris, and the acceleration signal of muscle contraction near the electrode was measured using a 3-axis acceleration sensor. A time- and frequency-domain analysis of the acceleration signals showed that the peak value of the signal increases with the increasing strength of the pulse burst and that the frequency spectra of the signals measured under various pulse bursts have characteristic frequencies (at approximately 2 Hz, 32 Hz, 45 Hz, and 55 Hz). Furthermore, we processed the data through multivariate nonlinear regression analysis and variance analysis and determined that the peak value of the signal scales with the logarithm to the base 10 of  $EN^x$ , where  $x$  is a value that scales with the logarithm to the base 10 of intraburst frequency ( $f$ ). These results indicate that for high-frequency nanosecond pulse treatment of solid tumors in or near muscles, when the field strength is relatively high, the intraburst frequency and the intraburst pulse number require appropriate selection to limit the strength of muscle contraction as much as possible.

## Keywords

high-frequency nanosecond pulse bursts, rabbit muscle contractions, dose effect, acceleration signal, spectrum distribution, function relation

Received: December 29, 2017; Revised: April 27, 2018; Accepted: June 13, 2018.

## Introduction

When treating tumors with a pulsed electric field, the undesirable side effect of muscle contraction inevitably arises.<sup>1,2</sup> Muscle contraction is caused by the direct stimulation of the surrounding muscles and indirect stimulation of the innervation nerve of the muscle.<sup>3-8</sup> For example, when a tumor is treated using a conventional microsecond pulse, the animal's muscles undergo a tetanic contraction, and the contraction frequency is consistent with the applied pulse frequency.<sup>7</sup> By injecting muscle relaxants, the degree of muscular tetanic contraction can be reduced to a certain extent but cannot be completely eliminated.<sup>9,10</sup> In the course of the treatment with nanosecond pulses, it is necessary to impose a pulsed electric field with a relatively high field strength into the tumor tissue by means of an electrode. The high field strength can easily cause surface

discharge on the surface of the target tissue.<sup>11</sup> These drawbacks adversely affect the smooth progress of the treatment process and the reliability of the treatment equipment.<sup>1,12,13</sup>

<sup>1</sup> State Key Laboratory of Power Transmission Equipment and System Security and New Technology, School of Electrical Engineering, Chongqing University, Chongqing, China

<sup>2</sup> Electric Power Research Institute State Grid Beijing Electric Power Company, Beijing, China

<sup>3</sup> First Affiliated Hospital, Chongqing Medical Science University, Chongqing, China

### Corresponding Author:

Yan Mi, PhD, School of Electrical Engineering, Chongqing University, No.174 Shazhengjie St., Shapingba Dist, Chongqing, People Republic of China.  
 Email: [miyan@cqu.edu.cn](mailto:miyan@cqu.edu.cn)



To address the abovementioned problems and combine the advantages of traditionally used microsecond pulses and nanosecond pulses, we proposed a new high-frequency nanosecond pulse form.<sup>14</sup> This new pulse form is proposed based on the following reasons. First, due to the disadvantage that a high electric field strength can easily cause surface discharge in the application of ordinary low-frequency nanosecond pulses, it is necessary to reduce the field strength. Lowering the field strength will reduce the effect of tumor treatment. According to the theoretically established relationship between biological effects and the field strength, pulse width, number of pulses, and pulse frequency proposed by Schoenbach *et al*,<sup>15</sup> the treatment effect can be improved by increasing the pulse frequency. Considering that the thermal effect is significant under continuous pulses, we propose the form of high-frequency nanosecond pulse bursts. In addition, the intraburst pulse numbers can be appropriately increased to improve the therapeutic effect.

This pulse is in the form of microsecond pulse-modulated nanosecond pulses and is expected to induce both apoptosis and to stimulate irreversible electroporation to achieve the purpose of treating a tumor. Our previous cell and animal experiments using high-frequency nanosecond pulses showed that this pulse form can effectively kill tumor cells and inhibit the growth of tumors *in vivo*.<sup>16</sup> These findings show that this type of pulse currently has a certain application potential for the treatment of tumors. To some extent, similar to high-frequency microsecond pulses,<sup>3,4,17,18</sup> the muscle contraction arising from high-frequency nanosecond pulses can be reduced by optimizing the pulse parameters. Therefore, to provide reference data for the selection of parameters for high-frequency nanosecond pulsed electric field treatment of tumors, it is necessary to study the effects of various high-frequency nanosecond pulse-burst parameters on muscle contraction.

At present, there is no systematic study of the strength of muscle contraction under the action of nanosecond pulses. Multiple experimental studies have been conducted on the phenomenon of muscle contraction under the action of a microsecond pulsed electric field. Arena *et al*<sup>3</sup> applied one hundred eighty 1000 to 4000 V/cm, 250 kHz/500 kHz high-frequency microsecond pulses and traditional microsecond pulses to the brain tissue of Fisher 344 rats. In the experiment, the muscle contraction signals were measured using an accelerometer sutured to the dorsum of each rat, and the muscle contraction signals measured in the 2 cases were compared. The results show that compared to conventional microsecond pulses, high-frequency microsecond pulses under each parameter do not produce detectable muscle contractions, but higher field strengths are required to achieve a similar tissue ablation area. Dong *et al*<sup>19</sup> performed rabbit liver ablation experiments using plate electrodes to apply high-frequency bipolar microsecond pulses with different pulse widths (1-50  $\mu$ s). In the experiment, an accelerometer is fixed on the belly of the rabbit to measure the intensity of muscle contraction. They found that high-frequency bipolar microsecond pulses with a pulse duration of 5  $\mu$ s and an electric field intensity of 2000/cm had a good ablation effect and caused a lesser extent of muscle

contractions in the animals. Miklavcic *et al*<sup>7</sup> used a train of eight 100- $\mu$ s rectangular pulses at various frequencies (1-5 kHz) to treat Wistar rats. The relationship between the pulse frequency and the muscle contractility was studied. With increasing frequency, the intensity of muscle contraction first increased and then decreased. At the same time, the efficiency of the *in vivo* treatments of tumors by electrochemotherapy are similar regardless of the pulse frequency applied. To systematically study the effects of multipulse parameters on muscle contraction and consider the fact that *in vivo* experiments can more accurately reflect muscle contraction strength when treating tumors, we explored the dose effect of an *in vivo* muscle contraction with various parameters of high-frequency nanosecond pulses.

Our study is based on the fact that muscle contraction occurs via the effect of leakage current. Therefore, we hypothesize that through pulse parameter adjustment, the muscle contraction strength in the actual tumor treatment can be limited to a low level. Many combinations of pulse-burst parameters exist that can be used to specify high-frequency nanosecond pulses. Therefore, we explored the influence of various parameters (field intensity, intraburst frequency, and intraburst pulse number) of high-frequency nanosecond pulse bursts on the muscle contraction of the biceps femoris in rabbits *in vivo*. In addition, the intensity of muscle contraction under a set of microsecond pulse parameters was measured as a control in this study. The results of this work can provide a reference for the subsequent selection of parameters for the treatment of tumors using high-frequency nanosecond pulsed electric fields.

## Materials and Methods

### Experimental Subjects

Seven male New Zealand white rabbits with body weights between 2.3 and 2.5 kg were used as the experimental subjects. The rabbits were obtained from the experimental animal center of Medical University of Chongqing (license number SYXK [Yu] 2012-0001) and were fed with a mixture of roughage and a nutrition diet in individually ventilated cages in a temperature-controlled room. All the protocols were approved by the Ethics Committee of The First Affiliated Hospital of Chongqing Medical University (approval number 20172101), and the experiment strictly enforced the relevant regulations on the management of experimental animals in China.

### Experimental Procedure In Vivo

Ten minutes before the treatment, the rabbits were anesthetized with pentobarbital sodium injection (30 mg/mL) at 1 mL/kg dose along the rabbit ear vein. The duration of anesthesia was approximately 1 hour. After the experiment was completed, the rabbits generally recovered from the anesthetic within approximately 20 minutes. After recovery, the rabbits exhibited a normal state of action, and no changes in the motor function of the stimulated thigh were observed.

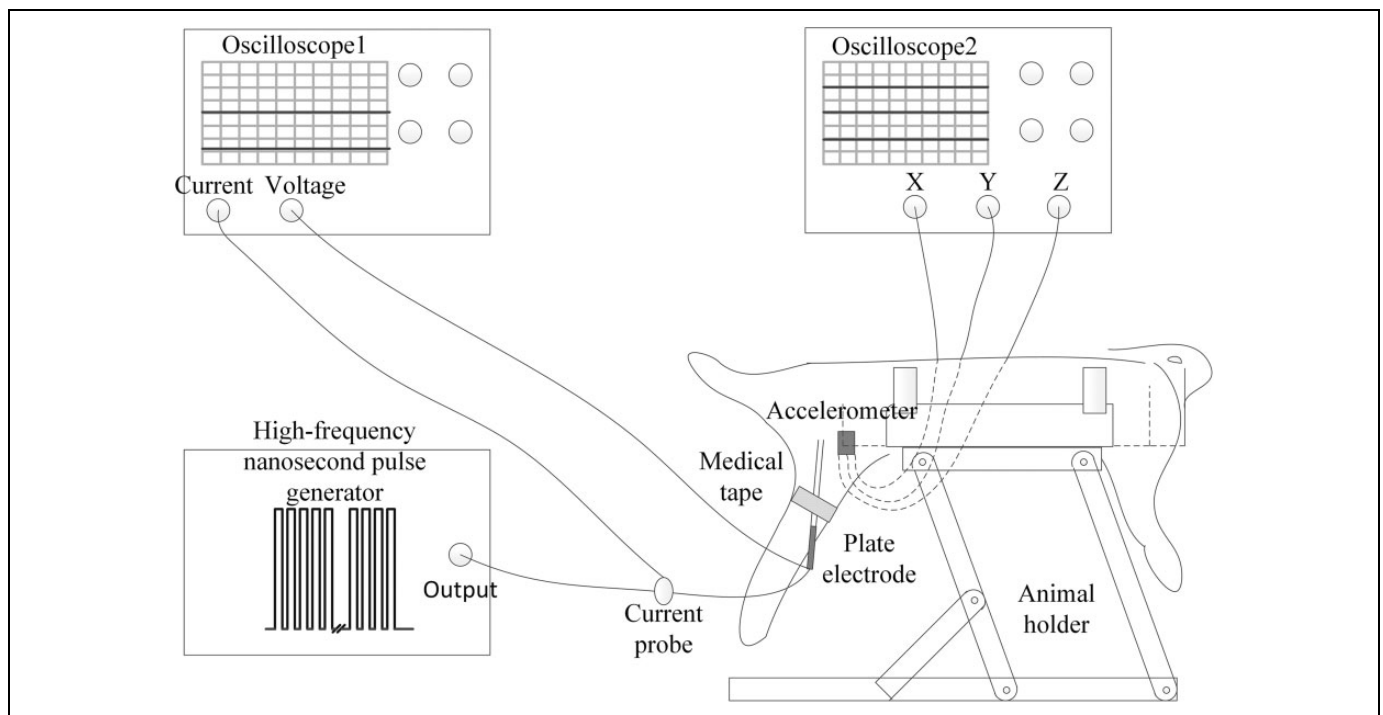


**Figure 1.** Diagram of the experimental system.

The selected pulsed electric field stimulation site was the rabbit thigh bicep skin surface. After the animal was anesthetized, the skin on one side of the thigh was shaved, and the remaining hair was removed using a depilatory. The animals were placed in a prone position on an experimental animal holder that constrained their limbs in a natural position. The surface skin of the biceps femoris was gently lifted and then clamped using a pair of plate electrodes. The selected electrode was a CUY650P3 plate electrode (BEX Co Ltd., Itabashi-Ku, Tokyo, Japan) with an electrode diameter of 3 mm. The electrode spacing was maintained at approximately 1.2 mm as measured using a Vernier caliper.

The measurement of muscle contraction signals can be achieved with a variety of sensors.<sup>20,21</sup> Here, we used an accelerometer (ADXL335; Analog Devices Inc, Norwood, Massachusetts) to measure the acceleration signal to assess the muscle contraction intensity. The ADXL335 is a 3-axis accelerometer that can be attached to the skin of the muscle using double-sided adhesive.<sup>20</sup> The original acceleration signal was collected and stored for subsequent analysis using a MDO3024 oscilloscope (Tektronix Inc, Beaverton, Oregon). Data acquisition lasted 20 seconds at a sampling frequency of 5 kHz. Figure 1 shows a diagram of the experimental system. To ensure repeatability of the experiment, the relative positions of the animal, the experimental animal holder, the plate electrode, and the acceleration sensor were kept fixed as much as possible.

The pulsed electric field was generated using a customized high-frequency nanosecond pulse generator that can output an independently controlled voltage, intraburst frequency, and

intraburst number of pulses according to the experiment specifications. The output voltages and currents were measured using a WavePro 760Zi-A oscilloscope (Teledyne LeCroy Inc, Chestnut Ridge, New York) with a PPE 5 kV high-voltage probe and a Pearson Current Probe 6600 (Pearson Electronics Inc, Palo Alto, California). In each experiment, we fixed the applied number of pulse bursts to 10 and the single pulse width to 250 nanoseconds. The variable pulse parameters were the field strength, intraburst frequency, and intraburst number of pulses. Figure 2 shows an experimental record of the pulse voltage and current waveform on the load.

### Pulse Protocols

According to our previous simulation results and related literature,<sup>22-24</sup> at a low field strength, a wide (hundreds of nanoseconds) nanosecond pulse is required to electroporate the cells to effectively kill the tumor cells. Relative to the 3 parameters of field strength, intraburst frequency, and intraburst pulse number, the pulse width selection range is narrow. Therefore, the pulse width of the high-frequency nanosecond pulse is fixed at 250 nanoseconds in this study. We used a 3-factor, 3-level comprehensive test method to perform the muscle contraction experiment. For each of the 3 parameters, 3 levels were selected (Table 1). Because, an intraburst frequency does not exist for 1 intraburst pulse, there are a total of 21 valid parameter combinations. Ten bursts of high-frequency nanosecond pulses were delivered to the skin for electric field stimulation at a 1 Hz interburst frequency. In the course of each experiment, the left hind leg or the right hind leg of each experimental rabbit were tested for all 21 parameter combinations. To

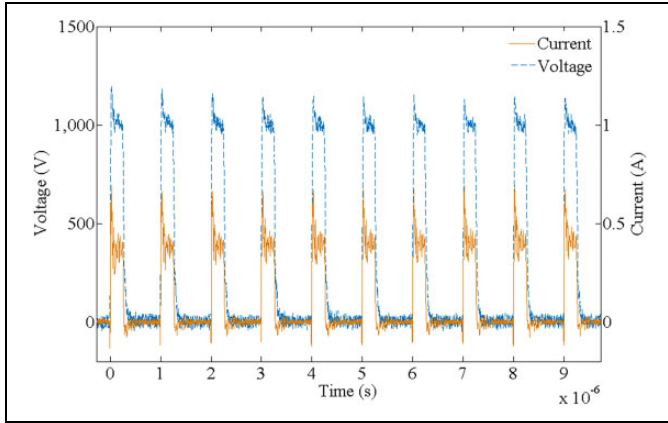


**Figure 2.** Measured voltage and current waveforms of the electric pulses.

**Table 1.** Experimental Factors and Levels.

Factor	Level		
	1	2	3
Field strength, $E/(kV \cdot cm^{-1})$	1	4	8
Intraburst frequency, $f/(Hz)$	10 k	100 k	1 M
Number of intraburst pulses, $N$	1	10	100

prevent errors caused by muscle fatigue on the experimental results, the interval between conducting 2 adjacent experiments on the same rabbit leg was 2 minutes.

In addition, to compare the relative strength of muscle contraction induced by high-frequency nanosecond pulse bursts and conventional microsecond pulses, we selected a set of microsecond pulse parameters (field strength 2 kV/cm, pulse width 100  $\mu s$ ) as a control. Accordingly, 10 microsecond pulses were applied to the rabbit skin for electric field stimulation at a frequency of 1 Hz in each experiment.

### Data Processing and Statistical Analysis

Because the original acceleration signal contained a substantial amount of useless noise interference, we processed the original acceleration signal using MATLAB to obtain a valid acceleration signal. In each experiment, 10 bursts of high-frequency nanosecond pulses under each group of parameters resulted in 10 acceleration signals. First, the signal was digitally filtered through a 1-200 Hz bandpass filter. Next, a 50 Hz digital frequency trap was used to filter out the power frequency signal interference. We then calculated the synthetic acceleration module value signal (subsequently referred to as the acceleration signal) as follows:

$$a = \sqrt{a_x^2 + a_y^2 + a_z^2} \quad (1)$$

where  $a_x$ ,  $a_y$ , and  $a_z$  are the recorded acceleration values in the  $x$ -,  $y$ -, and  $z$ -directions, respectively. Finally, the 10 acceleration signals were synchronously averaged to further reduce the

random signal interference. To compare the time-domain response of the acceleration signals under various pulse parameters, we set a threshold equal to 0.01 g to correspond to the onset of the averaged acceleration signals. The averaged acceleration signals with durations of 0.6 seconds were used for subsequent analysis. All data were statistically analyzed using SPSS version 19.0. The data are presented as the mean (standard deviation, [SD]) of 9 independent experiments, and the significance of the indexes between the different parameter groups was tested.

## Results

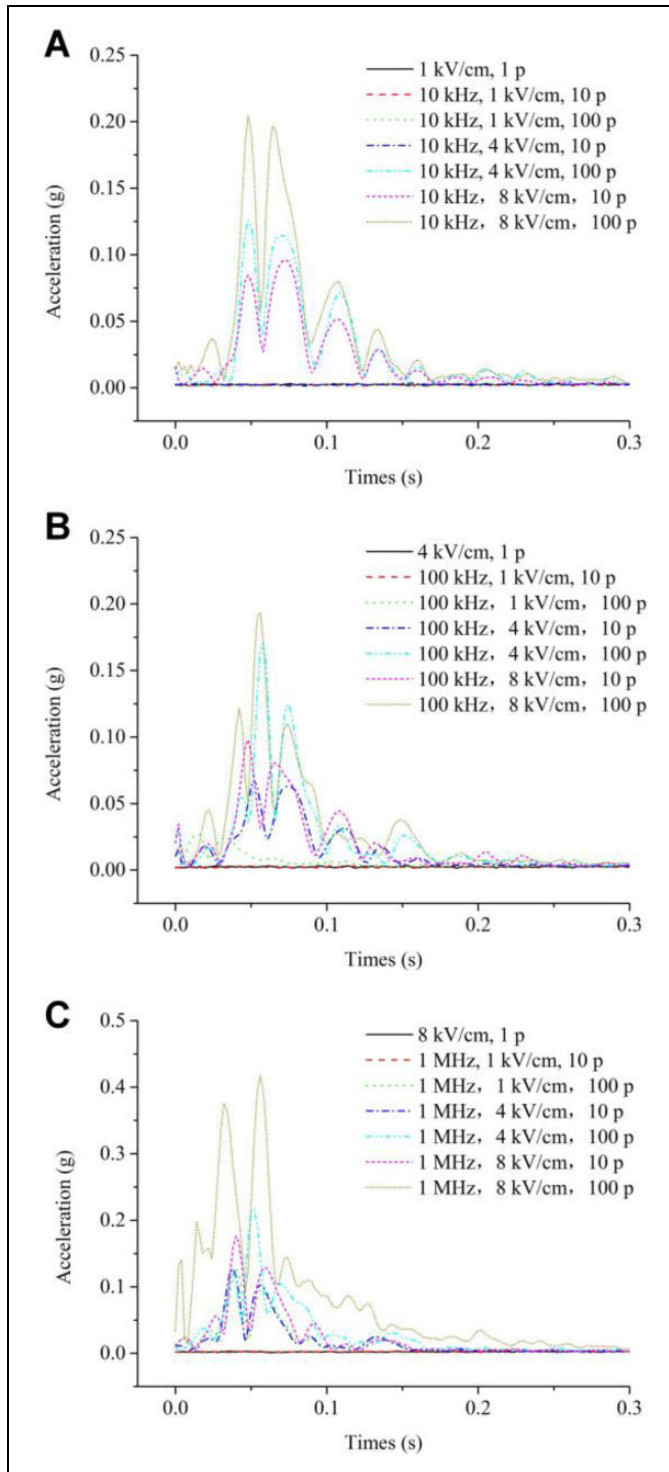
### Time-Domain Waveform of the Muscle Contraction Acceleration Signal

Figure 3 shows the time-domain signal of muscle contraction measured for all 21 groups of parameters in an independent experiment. No effective muscle contraction acceleration signal was detected in 8 parameter groups including the parameter group when the intraburst number of pulses was 1 (3 groups in total) and 5 other relatively weak parameter groups. For other parameter groups, the signals in Figure 3A and B look very similar and show an increase in Figure 3C. In addition to the 2 groups of parameters (the third set of parameters in the legend of Figure 3B and the seventh set of parameters in the legend of Figure 3C), the acceleration trend of the acceleration signal under different parameters is consistent. The deviations of the 2 lines are caused by the relatively low or strong amplitude of the muscle contraction signal, resulting in a different onset of the averaged acceleration signals. For other independent experiments, the acceleration signal also follows a similar pattern.

### Statistical Histogram of the Peak Value of the Acceleration Signal

The peak value of the acceleration signal was taken as the characteristic quantity to allow the influence of various pulse parameters on the muscle contraction strength to be analyzed. Figure 4A-C clearly shows that the mean value of the peak of the acceleration signal increases as the intraburst frequency, field strength, and intraburst number of pulses increase. However, the degree of increase differs at different levels. As shown in Figure 4, the peak value of the muscle contraction signal increases as the field strength increases, but the significant difference of this increase is weaker at higher intraburst frequencies; with the increase in the intraburst number of pulses, the peak value of muscle contraction signal also increases, but the significant difference of this increase is basically not affected by the intraburst frequency.

In addition, we measured the acceleration signal of muscle contraction under the action of a conventional microsecond pulse. The peak value statistics are shown in Figure 5. The peak value statistical results for the high-frequency nanosecond pulse burst with the strongest dose (250 ns, 1 MHz, 8 kV/cm,



**Figure 3.** Typical examples of acceleration signals of muscle contraction at various intraburst frequencies: (A) 10 kHz, (B) 100 kHz, and (C) 1 MHz. Each curve in the subfigure represents a single observation. Note that subfigure C is on a different scale on the ordinate.

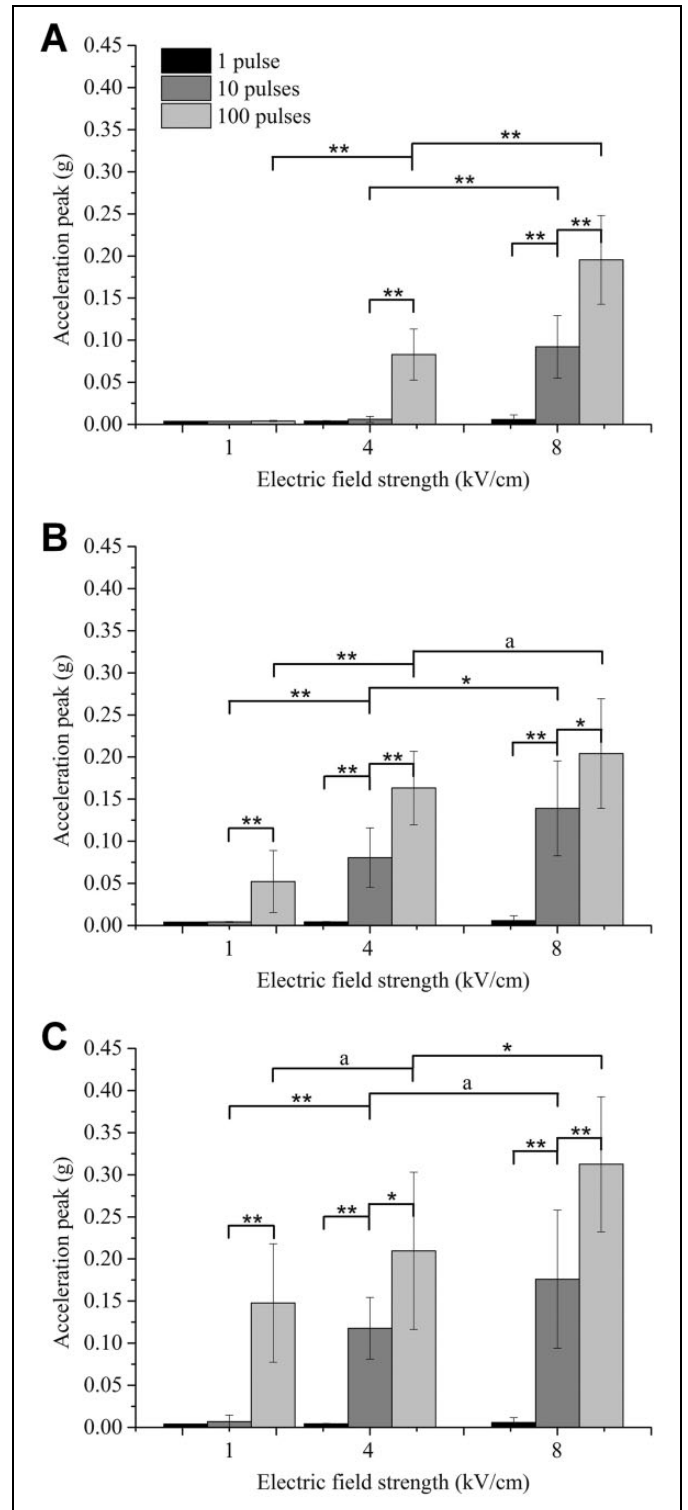


**Figure 4.** Peak value of the acceleration signal of the muscle contraction at various intraburst frequencies: (A) 10 kHz, (B) 100 kHz, and (C) 1 MHz. Note that the results corresponding to 1 intraburst pulse in subfigures A, B, and C are the same because an intraburst frequency does not exist in this case ( $*P < .05$ ,  $**P < .01$ ). 'a' represents no statistically significant difference.

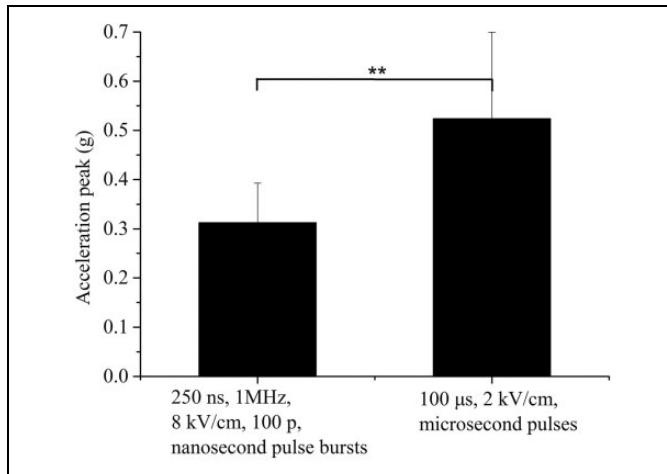


**Figure 5.** Comparison of the peak value of the acceleration signal of the muscle contraction under a high-frequency nanosecond pulse burst and a conventional microsecond pulse. The highest dose parameter and a typical parameter that is commonly used in irreversible electroporation were selected for the high-frequency nanosecond pulse burst and the microsecond pulse, respectively (\*\* $P < .01$ ).

100 p) was also presented for comparison. The peak value of the acceleration signal of the muscle contraction caused by the microsecond pulse is significantly larger than that of the high-frequency nanosecond pulse burst ( $P < .01$ ). Because the pulse parameters used in the experiment are limited, the relationship between the muscle contraction strength and the parameters can be obtained by numerical interpolation of the existing experimental data. Figure 6A-C shows that there is no definite change in the trend of the peak value of the acceleration signal with the increase in the electric field strength or the intraburst pulse number at the same intraburst frequency.

According to the 3-dimensional (3D) relationship, one can also obtain the contour line for a certain value of acceleration peak (Figure 7A). During the course of the experiment, when the peak of the acceleration caused by muscle contraction in rabbits was  $<0.15$  g, weak muscle contraction or no visible muscle contraction was observed during the course of the experiment. The region below the contour is the parameter range in which the peak value of the acceleration signal is less than the threshold value. Furthermore, we obtained a 3D contour surface as shown in Figure 7B.

### Acceleration Signal in the Frequency Domain Under Various Pulse Parameters

The amplitude spectrum of the acceleration signal (Figure 3) under different parameters can be obtained via fast Fourier transform as shown in Figure 8. In the frequency domain, the trends of the acceleration signals are consistent. In addition, the acceleration signal frequency is distributed primarily below 60 Hz. Except for the slight difference in the results for the 2

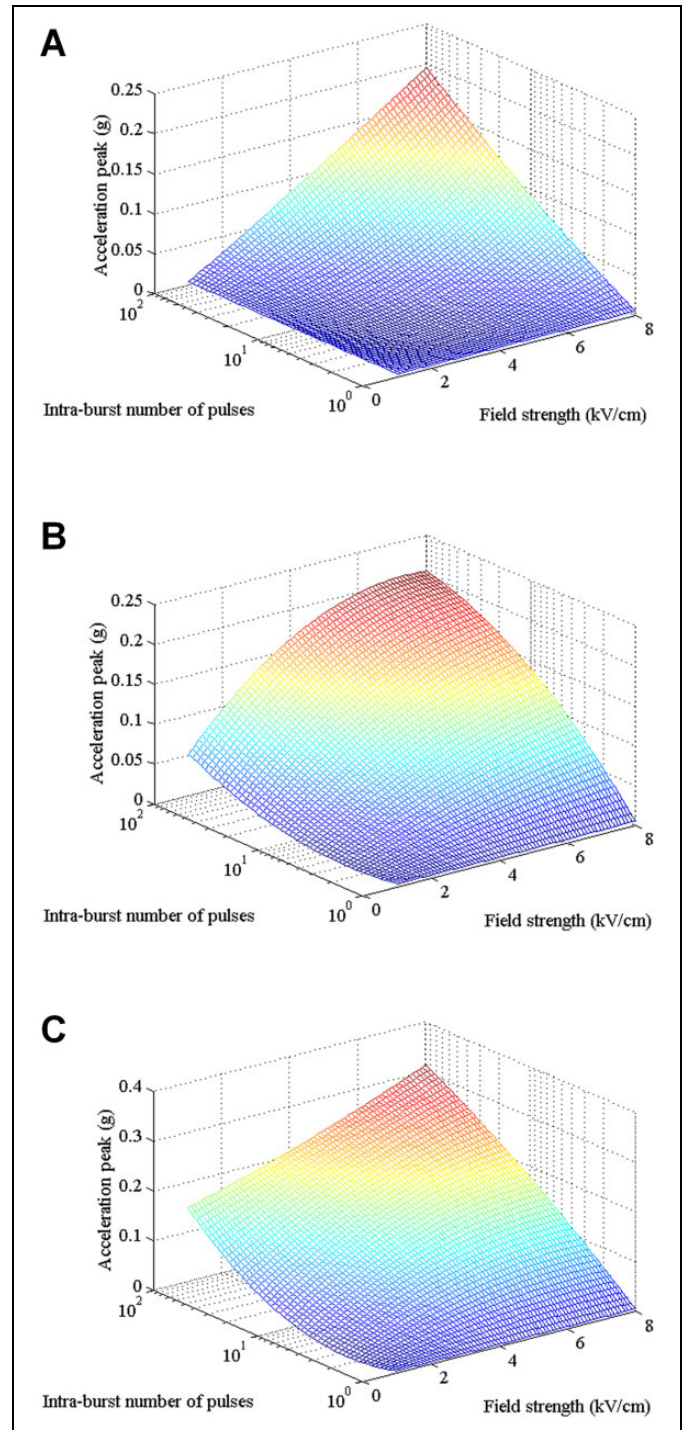


**Figure 6.** Three-dimensional relationship among the peak value of the acceleration signal of the muscle contraction, the electric field intensity and the intraburst number of pulses at various intraburst frequencies: (A) 10 kHz, (B) 100 kHz, and (C) 1 MHz.

parameters mentioned above, the amplitude spectrum of the acceleration signal contains characteristic frequencies at approximately 2 Hz, 32 Hz, 45 Hz, and 55 Hz. These results show that the high-frequency nanosecond pulse-induced muscle contraction is determined primarily by the resonance

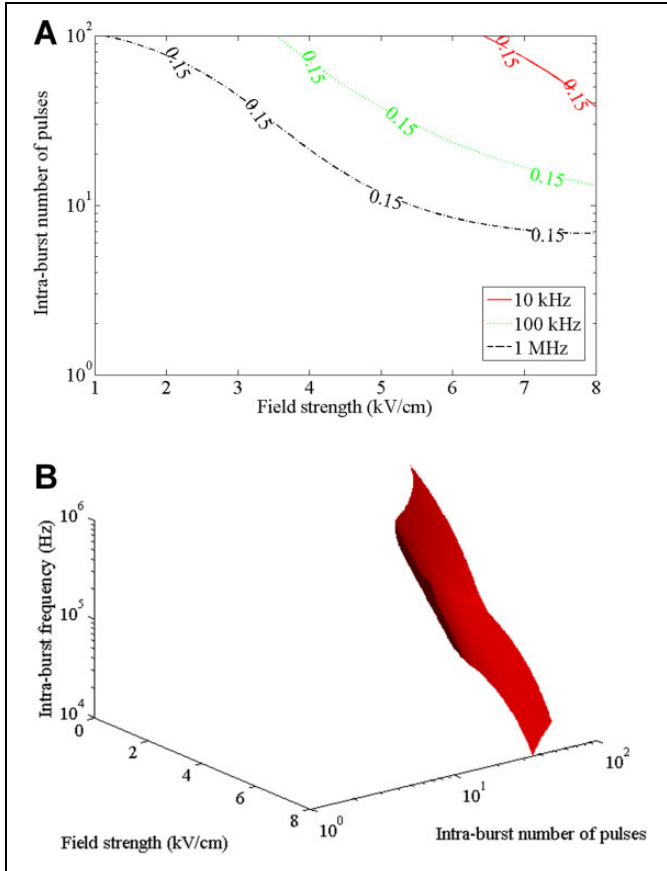


**Figure 7.** Contour lines and 3D contour surface for the peak value of 0.15 g of the acceleration signal of the muscle contraction under various electric field intensities, intraburst frequencies, and intraburst number of pulses: (A) contour lines and (B) 3D contour surface.

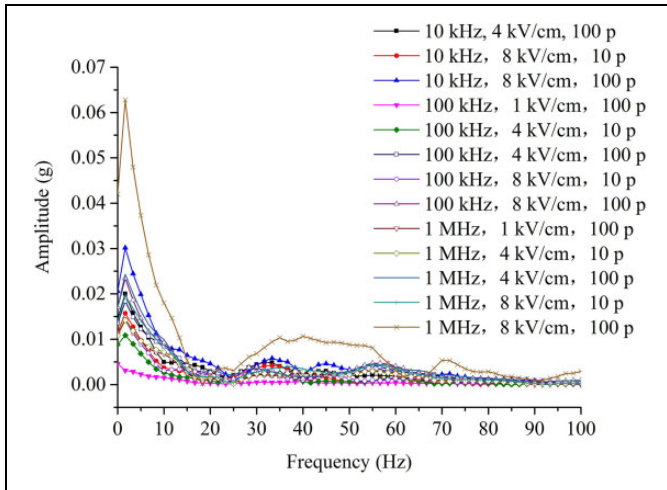


**Figure 8.** Amplitude spectrum of the acceleration signal (Figure 3) of the muscle contraction for the high-frequency nanosecond pulse bursts of various parameters.

frequencies of the muscle tissue.<sup>20,25,26</sup> For other independent experiments, the amplitude spectrum of the acceleration signal follows a similar law.

### Relationship Between the Peak Value of the Acceleration Signal of the Muscle Contraction and the Dose of the Pulsed Electric Field

To further analyze the effect of the 3 parameters on the effect of muscle contraction, we used the multiparameter variable method to quantitatively analyze the trend of muscle contraction acceleration intensity and the 3 parameters. Here, we assume that the peak of the acceleration signal caused by muscle contraction at the same intraburst frequency is proportional to the injected pulse energy  $EN^{(1/2)}$ . Taking the logarithm of pulse energy as the abscissa, we plot the relationship curve under intraburst frequencies of 10 kHz, 100 kHz, and 1 MHz (Figure 9A). The peak value of the acceleration signal increases with increasing pulse-injection energy at the frequency of the same intraburst frequency; however, the proportional relationship between the peak value of the acceleration signal and the injected energy is not easily detected. In addition, a threshold effect of muscle contraction is observed; that is, the effective muscle contraction signal is detected when the pulse-injected energy exceeds a certain value. Similarly, using the logarithm of the pulse charge  $EN^{(1)}$  as the abscissa, we also plot the relationship curve (Figure 9B); the proportional relationship between the peak value of the acceleration signal and the amount of injected pulse charge is less pronounced.

We assume that the peak of the acceleration signal caused by muscle contraction is proportional to the pulse-injection dose,  $EN^x$ , where the index of the intraburst number of pulses  $x$  is a variable related to the intraburst frequency. According to the relevant literatures,<sup>15,27</sup> the pulse-injection dose here represents an electrical impact dose factor. Furthermore, we assume that the following function relation is satisfied:

$$a = x \times \log(EN^{(y \times \log(f))}) + z \quad (2)$$

where  $x$ ,  $y$ , and  $z$  are undetermined coefficients. The derivation of this equation is based on the combination of the experimental results and characteristics of the parameter values. Considering that both the values of intraburst frequency ( $f$ ) and intraburst pulse number ( $N$ ) have a 10-fold relationship, we take the logarithm to the base 10 of the intraburst frequency as well as the pulse-injection dose  $EN^x$ . Moreover, from the experimental results obtained, we found that the peak value of the acceleration signal and the pulse-injection dose in logarithm form can be well fitted by a linear relationship. Using MATLAB, the multivariate nonlinear regression of the peak data of the effective acceleration signal can be fitted to obtain the quantitative function:

$$a = 0.1818 \times \log(EN^{(0.1174 \times \log(f))}) - 0.1434 \quad (3)$$

Using the pulse-injection dose in relation to the intraburst frequency  $EN^{(0.1174 \times \log(f))}$  as the abscissa, we plot the relationship curve (Figure 9C). The experimental data at different frequencies are well fitted by the function (the  $R^2$  is .8524), and the distribution of experimental data at different frequencies is also relatively concentrated.

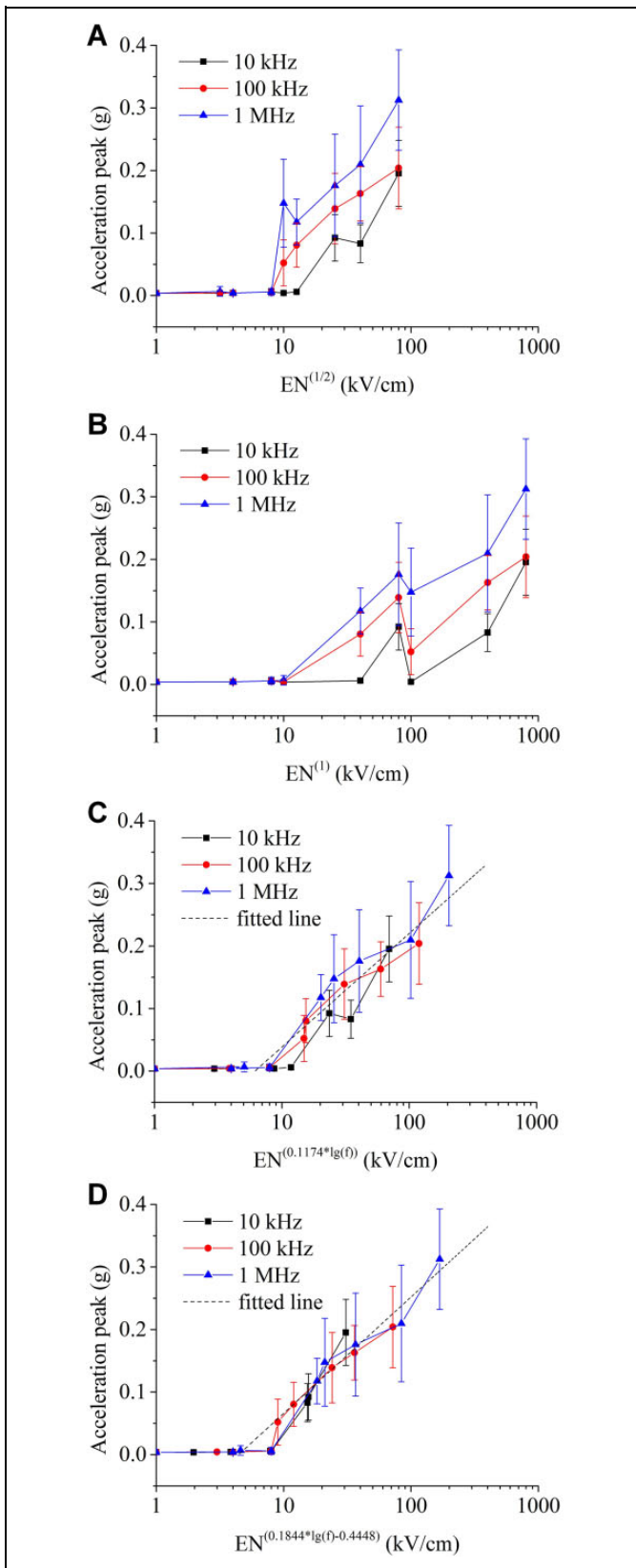


**Figure 9.** The relationship between the peak value of the acceleration signal of the muscle contraction and the pulsed electric field dose when using (A) pulse-injection energy, (B) pulse-injection charge, (C) pulse-injection dose  $EN^{(0.1174*\log(f))}$ , and (D) pulse-injection dose  $EN^{(0.1844*\log(f)-0.4448)}$  as the abscissa.

The N-index for the function fitting is linearly related to the logarithm of the intraburst frequency ( $f$ ). When other indices are selected, a better-fitting relationship with the experimental data can be obtained. If a coefficient is added to the exponent of  $N$ , the fitting function becomes

$$a = x \times \log(EN^{(y_1 \times \log(f) + y_2)}) + z \quad (4)$$

By performing multiple nonlinear regression for the peak data of the effective acceleration signal, the improved fitting function formula is obtained:

$$a = 0.1861 \times \log(EN^{(0.1844 \times \log(f) - 0.4448)}) - 0.1202 \quad (5)$$

Figure 9D shows that the experimental data of the acceleration signal peak coincide better with the fitting curve (the  $R^2$  is .9309). Correspondingly, Table 2 shows the statistical data arranged according to the functional relationship for various intraburst frequencies.

A multiple-factor analysis of variance can be performed on all 27 groups of data to further analyze the main and interaction effect of the factors as shown in Table 3. Except for the lack of a significant interaction effect between the field strength and the intraburst frequency, the main effects of the 3 factors and the second- and third-order interaction effects are significant. The  $F$ -test value of the intraburst number of pulses is the largest, which indicates that the main effect is the largest, followed by the field intensity and the intraburst pulse frequency.

## Discussion

Relative to the microsecond pulses with a pulse width of 50 to 100 microseconds, the use of shorter (submicrosecond or even nanosecond) pulses can significantly inhibit muscle contraction.<sup>4,17</sup> For a pulse form of high-frequency nanosecond pulse bursts, appropriate parameter selection is particularly important for improving efficacy in the treatment of tumors while minimizing muscle contractions.

An acceleration sensor can be used to evaluate the characteristics of muscle contraction, the acquisition of motion information, the measurement of the vibration of the object, and so on.<sup>20,25,26,28-31</sup> Based on this background, we explored the dose effect of various parameters of high-frequency nanosecond pulse bursts on the muscle contraction strength. We measured the muscle contraction acceleration signals induced by electric stimulation on the surface skin of rabbits' biceps femoris *in vivo*. Based on the abovementioned experimental results and analysis, we conclude that the muscle contraction strength increases with increasing electric field strength, intraburst number of pulses, and intraburst frequency. This result is different from that of the study by Miklavcic *et al* who found that the intensity of muscle contraction first increased and then decreased with increasing pulse frequency.<sup>7</sup> This difference may be caused by the different pulse protocols applied. The duration of a single high-frequency nanosecond burst used in this study is relatively short (less



**Table 2.** The Peak Value Statistics of the Acceleration Signal of Muscle Contraction.

10 kHz		100 kHz		1 MHz	
$EN^{(0.2927)}/(kV \cdot cm^{-1})$	$a/(g)$	$EN^{(0.4770)}/(kV \cdot cm^{-1})$	$a/(g)$	$EN^{(0.6613)}/(kV \cdot cm^{-1})$	$a/(g)$
1	0.0039 (0.0002)	1	0.0039 (0.0002)	1	0.0039 (0.0002)
1.962	0.0037 (0.0002)	2.999	0.0042 (0.0006)	4	0.0041 (0.0005)
3.849	0.0041 (0.0006)	4	0.0041 (0.0005)	4.585	0.0068 (0.0077)
4	0.0041 (0.0005)	8	0.0058 (0.0057)	8	0.0058 (0.0057)
7.848	0.0060 (0.0036)	8.995	0.0521 (0.0367)	18.338	0.1176 (0.0366)
8	0.0058 (0.0057)	11.997	0.0805 (0.0352)	21.018	0.1477 (0.0703)
15.696	0.0922 (0.0371)	23.993	0.1390 (0.0563)	36.677	0.1760 (0.0821)
15.398	0.0830 (0.0304)	35.980	0.1630 (0.0437)	84.073	0.2097 (0.0934)
30.796	0.1954 (0.0527)	71.960	0.2040 (0.0651)	168.147	0.3124 (0.0802)

**Table 3.** Tests of Between-Subject Effects.

Source	Type III Sum of Squares	Degree of Freedom ( <i>df</i> )	Mean Square	<i>F</i> -statistic	Sig.
Corrected Model	1.853	26	0.071	42.442	.000
Intercept	1.375	1	1.375	819.093	.000
Electric field strength (E)	.412	2	0.206	122.645	.000
Number of intraburst pulses (N)	.895	2	0.447	266.369	.000
Intraburst frequency (f)	.173	2	0.086	51.419	.000
E × N	.209	4	0.052	31.094	.000
E × f	.013	4	0.003	2.007	.095
N × f	.119	4	0.030	17.789	.000
E × N × f	.032	8	0.004	2.384	.018
Error	.363	216	0.002		
Total	3.591	243			
Corrected Total	2.216	242			

than 10 milliseconds), and muscle contraction generally reflects a cumulative effect that increases with increasing pulse frequency. Thus, as the intraburst frequency increases, the peak of the acceleration signal caused by muscle contraction is expected also to increase. However, the frequency spectra of the acceleration signal measured under different pulse bursts are similar. This finding demonstrates that high-frequency nanosecond pulse-induced muscle contraction is determined primarily by the resonance frequencies of the muscle tissue.<sup>20,25,26</sup>

A multiparameter regression analysis shows that the muscle contraction strength under high-frequency nanosecond pulse bursts can be approximated as a function of the frequency-dependent pulse-injection dose  $EN^x$ . The higher the intraburst frequency, the larger the value of the exponent  $x$ . If linear regression fitting is performed on the peak value of the effective acceleration signal, then a similar fitness can be achieved. However, the intraburst frequency has no effect on the pulse form in the case of a single intraburst pulse, indicating that the intraburst frequency ( $f$ ) is a better choice as an exponent. In

addition, a saturation effect of muscle contraction is clearly detected as reflected in the logarithm of the pulse-injection dose in the formula. According to the relationship between these 3 parameters, we can better guide the selection of pulse parameters in the treatment of tumors with high-frequency nanosecond pulse bursts.

## Conclusion

According to the study results, we draw the following conclusions: with increasing field intensity, intraburst frequency, and intraburst pulse number, the muscle contraction strength increases, whereas muscle contraction does not occur with weak parameters. The amplitude spectra of the acceleration signal are consistent and are distributed primarily below 60 Hz. From a quantitative perspective, we obtained a dose relationship between the pulse-burst parameters and the animal muscle contraction strength. The results demonstrated that muscle contraction under a high-frequency nanosecond pulse burst mainly reflects a cumulative effect. With the increase in the pulse dose, the muscle contraction intensity increases; however, a certain saturation effect exists. The results of this study provide a reference for the selection of a high-frequency nanosecond pulsed electric field in the treatment of tumors and indicate that the pulse parameters should be considered systematically in pulse protocols designed to minimize the strength of muscle contraction.

## Declaration of Conflicting Interests

The author(s) declared no potential conflicts of interest with respect to the research, authorship, and/or publication of this article.

## Funding

The author(s) disclosed receipt of the following financial support for the research, authorship, and/or publication of this article: This work was supported in part by the National Natural Science Foundation of China (51477022, 51321063), the National Science Foundation Project of CQ CSTC (cstc2014jcyjA90001, cstc2016jcyjA0500), and the National "111" Project of China (B08036).

## References

1. Golberg A, Yarmush ML. Nonthermal irreversible electroporation: fundamentals, applications, and challenges. *IEEE Trans Biomed Eng.* 2013;60(3):707-714.
2. Rubinsky B, Onik G, Mikus P. Irreversible electroporation: a new ablation modality—clinical implications. *Technol Cancer Res Treatment.* 2007;6(1):37-48.
3. Arena CB, Sano MB, Rossmeisl JH Jr, et al. High-frequency irreversible electroporation (H-FIRE) for non-thermal ablation without muscle contraction. *BioMed Eng Online.* 2011;10(1):1-21.
4. Sano MB, Arena CB, Bittleman KR, et al. Bursts of bipolar microsecond pulses inhibit tumor growth. *Sci Rep.* 2015;5:14999.
5. Pucihar G, Mir LM, Miklavčič D. The effect of pulse repetition frequency on the uptake into electroporated cells in vitro with possible applications in electrochemotherapy. *Bioelectrochemistry.* 2002;57(2):167-172.
6. Vikulova NA, Katsnelson LB, Kursanov AG, Solovyova O, Markhasin VS. Mechano-electric feedback in one-dimensional model of myocardium. *J Math Biol.* 2016;73(2):335-366.
7. Miklavcic D, Pucihar G, Pavlovec M, et al. The effect of high frequency electric pulses on muscle contractions and antitumor efficiency in vivo for a potential use in clinical electrochemotherapy. *Bioelectrochemistry.* 2005;65(2):121-128.
8. Ribarić S, Stefanovska A, Brzin M, Kogovsek M, Kroselj P. Biochemical, morphological, and functional changes during peripheral nerve regeneration. *Mol Chem Neuropathol.* 1991;15(2):143-157.
9. Martin RC, Schwartz E, Adams JA, Farah I, Derhake BM. Intraoperative anesthesia management in patients undergoing surgical irreversible electroporation of the pancreas, liver, kidney, and retroperitoneal tumors. *Region Anesth Pain Med.* 2015;5(3):e22786.
10. Ball C, Thomson KR, Kavvoudias H. Irreversible electroporation: a new challenge in “out of operating theater” anesthesia. *Anesth Analg.* 2010;110(5):1305-1309.
11. Nuccitelli R, Huynh J, Lui K, et al. Nanoelectroablation of human pancreatic carcinoma in a murine xenograft model without recurrence. *Int J Cancer.* 2013;132(8):1933-1939.
12. Breton M, Mir LM. Microsecond and nanosecond electric pulses in cancer treatments. *Bioelectromagnetics.* 2012;33(2):106-123.
13. Maor E, Ivorra A, Rubinsky B. Non thermal irreversible electroporation: novel technology for vascular smooth muscle cells ablation. *Plos One.* 2009;4(3):e4757.
14. Yan M, Rui S, Li C, et al. Multi-parametric study of temperature and thermal damage of tumor exposed to high-frequency nanosecond-pulsed electric fields based on finite element simulation. *Med Biol Eng Comput.* 2017;55(7):1109-1122.
15. Schoenbach KH, Joshi RP, Beebe SJ, et al. A scaling law for membrane permeabilization with nanopulses. *IEEE Trans Dielect Elect Insul.* 2009;16(5):1224-1235.
16. Zhang B, Kuang D, Tang X, et al. Effect of low-field high-frequency nsPEFs on the biological behaviors of human A375 melanoma cells. *IEEE Trans Biomed Eng.* 2017;PP(99):1-1.
17. Long G, Shires PK, Plescia D, Beebe SJ, Kolb JF, Schoenbach KH. Targeted tissue ablation with nanosecond pulses. *IEEE Trans Biomed Eng.* 2011;58(8):2161-2167.
18. Shankayi Z, Firoozabadi SM, Hassan ZS. Optimization of electric pulse amplitude and frequency in vitro for low voltage and high frequency electrochemotherapy. *J Membr Biol.* 2014;247(2):147-154.
19. Dong S, Yao C, Zhao Y, et al. Parameters optimization of bipolar high frequency pulses on tissue ablation and inhibiting muscle contraction. *IEEE Trans Dielect Electr Insul.* 2018;25(1):207-216.
20. Uchiyama T, Shinohara K. Comparison of displacement and acceleration transducers for the characterization of mechanics of muscle and subcutaneous tissues by system identification of a mechanomyogram. *Med Biol Eng Comput.* 2013;51(1-2):165-173.
21. Rogers WR, Merritt JH, Comeaux JA, et al. Strength-duration curve for an electrically excitable tissue extended down to near 1 nanosecond. *IEEE Trans Plas Sci.* 2004;32(4):1587-1599.
22. Mi Y, Xu J, Tang X, et al. Electroporation simulation of a multicellular system exposed to high-frequency 500 ns pulsed electric fields. *IEEE Trans Dielect Elect Insul.* 2018;24(6):3985-3994.
23. Nuccitelli R, Pliquett U, Chen X, et al. Nanosecond pulsed electric fields cause melanomas to self-destruct. *Biochem Biophys Res Commun.* 2006;343(2):351-360.
24. Chen X, Swanson RJ, Kolb JF, Nuccitelli R, Schoenbach KH. Histopathology of normal skin and melanomas after nanosecond pulsed electric field treatment. *Melanoma Res.* 2009;19(6):361-371.
25. Uchiyama T, Sakai H. System identification of evoked mechanomyogram from abductor pollicis brevis muscle in isometric contraction. *Med Biol Eng Comput.* 2013;51(12):1349-1355.
26. Islam MA, Sundaraj K, Ahmad RB, Ahamed NU. Mechanomyography sensor development, related signal processing, and applications: a systematic review. *IEEE Sens J.* 2013;13(7):2499-2516.
27. Romeo S, Wu YH, Levine ZA, Gundersen MA, Vernier PT. Water influx and cell swelling after nanosecond electroporation. *Biochim Biophys Acta.* 2013;1828(8):1715-1722.
28. Silva J, Chau T. A mathematical model for source separation of MMG signals recorded with a coupled microphone-accelerometer sensor pair. *IEEE Trans Biomed Eng.* 2005;52(9):1493-1501.
29. Klunder M, Feuer R, Amend B, et al. Eliminating pulse-induced artifacts in urethral pressure data. *Conf Proc IEEE Eng Med Biol Soc.* 2015:2779-2783.
30. Khan ZA, Zabit U, Bernal OD, et al. Adaptive cancellation of parasitic vibrations affecting a self-mixing interferometric laser sensor. *IEEE Trans Instrum Meas.* 2017;66(2):332-339.
31. Menotti F, Labanca L, Laudani L, Giombini A, Pigozzi F, Macaluso A. Activation of neck and low-back muscles is reduced with the use of a neck balance system together with a lumbar support in urban drivers. *Plos One.* 2015;10(10):e0141031.